

Sideband Cooling Micromechanical Motion to the Quantum Ground State

J. D. Teufel,¹ T. Donner,² Dale Li,¹ J. W. Harlow,^{2,3} M. S. Allman,¹ K. Cicak,¹
A. J. Sirois,¹ J. D. Whittaker,¹ K. W. Lehnert,^{2,3} and R. W. Simmonds¹

¹*National Institute of Standards and Technology, Boulder, CO 80305, USA*

²*JILA, National Institute of Standards and Technology and the University of Colorado, Boulder, CO 80309, USA*

³*Department of Physics, University of Colorado, Boulder, Colorado 80309, USA*

The advent of laser cooling techniques revolutionized the study of many atomic-scale systems. This has fueled progress towards quantum computers by preparing trapped ions in their motional ground state [1], and generating new states of matter by achieving Bose-Einstein condensation of atomic vapors [2]. Analogous cooling techniques [3, 4] provide a general and flexible method for preparing macroscopic objects in their motional ground state, bringing the powerful technology of micromechanics into the quantum regime. Cavity opto- or electro-mechanical systems achieve sideband cooling through the strong interaction between light and motion [5–15]. However, entering the quantum regime, less than a single quantum of motion, has been elusive because sideband cooling has not sufficiently overwhelmed the coupling of mechanical systems to their hot environments. Here, we demonstrate sideband cooling of the motion of a micromechanical oscillator to the quantum ground state. Entering the quantum regime requires a large electromechanical interaction, which is achieved by embedding a micromechanical membrane into a superconducting microwave resonant circuit. In order to verify the cooling of the membrane motion into the quantum regime, we perform a near quantum-limited measurement of the microwave field, resolving this motion a factor of 5.1 from the Heisenberg limit [3]. Furthermore, our device exhibits strong-coupling allowing coherent exchange of microwave photons and mechanical phonons [16]. Simultaneously achieving strong coupling, ground state preparation and efficient measurement sets the stage for rapid advances in the control and detection of non-classical states of motion [17, 18], possibly even testing quantum theory itself in the unexplored region of larger size and mass [19]. The universal ability to connect disparate physical systems through mechanical motion naturally leads towards future methods for engineering the coherent transfer of quantum information with widely different forms of quanta.

Mechanical oscillators that are both decoupled from their environment (high quality factor Q) and placed in the quantum regime could allow us to explore quantum mechanics in entirely new ways [17–21]. For an oscillator to be in the quantum regime, it must be possible to prepare it in its ground state, to arbitrarily manipulate its quantum state, and to detect its state near the Heisenberg limit. In order to prepare an oscillator in its ground state, its tempera-

ture T must be reduced such that $k_B T < \hbar \Omega_m$, where Ω_m is the resonance frequency of the oscillator, k_B is Boltzmann's constant, and \hbar is the reduced Planck's constant. While higher resonance frequency modes (> 1 GHz) can meet this cooling requirement with conventional refrigeration ($T < 50$ mK), these stiff oscillators are difficult to control and to detect within their short mechanical lifetimes. One unique approach using passive cooling has successfully overcome these difficulties by using a piezoelectric dilatation oscillator coupled to a superconducting qubit [22]. Unfortunately, this method is incompatible with the broad range of lower frequency, high Q , flexural mechanical modes. In order to take advantage of the attractive mechanical properties of these oscillators, an alternative active cooling method is required, one that can reduce the oscillator's temperature below that of the surrounding environment.

Cavity opto- or electro-mechanical systems [4] naturally offer a method for both detecting mechanical motion and cooling a mechanical mode to its ground state [23, 24]. An object whose motion alters the resonance frequency ω_c of an electromagnetic cavity experiences a radiation pressure force governed by the parametric interaction Hamiltonian: $\hat{H}_{\text{int}} = \hbar G \hat{n} \hat{x}$, where $G = d\omega_c/dx$, \hat{n} is the cavity photon number, and \hat{x} is the displacement of the mechanical oscillator. By driving the cavity at a frequency ω_d , the oscillator's motion produces upper and lower sidebands at $\omega_d \pm \Omega_m$. Because these sideband photons are inelastically scattered from the drive field, they provide a way to exchange energy with the oscillator. If the drive field is optimally detuned below the cavity resonance $\Delta \equiv \omega_d - \omega_c = -\Omega_m$, photons will be preferentially up-converted to ω_c because the photon density of states is maximal there (Fig 1b). When an up-converted photon leaves the cavity, it removes the energy of one mechanical quantum (one phonon) from the motion. Thus, the mechanical oscillator is damped and cooled via this radiation-pressure force. Because the mechanical motion is encoded in scattered photons exiting the cavity, a quantum-limited measurement of this photon field provides a near Heisenberg-limited detection of mechanical motion [25].

While there has been substantial progress in cooling mechanical oscillators with radiation pressure forces, sideband cooling to the quantum mechanical ground state has been an outstanding challenge. Cavity optomechanical systems have realized very large sideband cooling rates [8–

12, 14, 15]; however, these rates are not sufficient to overcome the larger thermal heating rates of the mechanical modes. Because electromechanical experiments use much lower-energy photons [5–7, 13], they are naturally compatible with operation below 100 mK, but have consequently suffered from weak electromechanical interactions and inefficient detection of the photon fields.

Here, we present a cavity electromechanical system where a flexural mode of a thin aluminum membrane is parametrically coupled to a superconducting microwave resonant circuit. Unlike previous microwave systems, this device achieves large electromechanical coupling by concentrating nearly all the microwave electric fields near the mechanical oscillator [16]. The oscillator is a 100 nm thick aluminum membrane with a diameter of 15 μm , suspended 50 nm above a second aluminum layer on a sapphire substrate [26] (see Fig. 1). These two metal layers form a variable parallel-plate capacitor that is shunted by a 12 nH spiral inductor. This combination of capacitor and inductor creates a microwave cavity whose resonance frequency depends on the mechanical displacement of the membrane and is centered at $\omega_c = 2\pi \times 7.54$ GHz. The device is operated in a dilution refrigerator at 15 mK, where aluminum is superconducting, and the microwave cavity has a total energy decay rate of $\kappa \approx 2\pi \times 200$ kHz. As expected from the dimensions of the membrane, $\Omega_m = 2\pi \times 10.56$ MHz, and we find an intrinsic damping rate of $\Gamma_m = 2\pi \times 32$ Hz, resulting in a mechanical quality factor $Q_m = \Omega_m/\Gamma_m = 3.3 \times 10^5$. The oscillator mass $m = 48$ pg implies that the zero-point motion is $x_{z\text{p}} = \sqrt{\hbar/(2m\Omega_m)} = 4.1$ fm. With a ratio of $\Omega_m/\kappa > 50$, our system is deep in the resolved-sideband regime and perfectly suited for sideband cooling to the mechanical ground state [23, 24].

To measure the mechanical displacement, we apply a microwave field, which is detuned below the cavity resonance frequency by $\Delta = -\Omega_m$, through heavily attenuated coaxial lines to the feed line of our device. The upper sideband at ω_c is amplified with a custom-built Josephson parametric amplifier (JPA) [27, 28] followed by a low-noise cryogenic amplifier, demodulated at room temperature, and finally monitored with a spectrum analyzer. The thermal motion of the membrane creates an easily resolvable peak in the microwave noise spectrum. As described previously [28], this measurement scheme constitutes a nearly shot-noise-limited microwave interferometer with which we can measure mechanical displacement with minimum added noise close to fundamental limits.

In order to calibrate the demodulated signal to the membrane's motion, we measure the thermal noise spectrum while varying the cryostat temperature (Fig. 1c). Here a weak microwave drive (~ 3 photons in the cavity) is used in order to ensure that radiation pressure damping and cooling effects are negligible. When $\Omega_m \gg \kappa \gg \Gamma_m$ and $\Delta = -\Omega_m$, the displacement spectral density S_x is related to the observed microwave noise spectral density S by: $S_x = 2(\kappa\Omega_m/G\kappa_{\text{ex}})^2 S/P_o$, where κ_{ex} is the cou-

pling rate between the cavity and the feed line, and P_o is the power of the microwave drive at the output of the cavity. According to equipartition, the area under the resonance curve of displacement spectral density S_x must be proportional to the effective temperature of the mechanical mode. This calibration procedure allows us to convert the sideband in the microwave power spectral density to a displacement spectral density and to extract the thermal occupation of the mechanical mode. In Fig. 1c we show the number of thermal quanta in the mechanical resonator as a function of T . The linear dependence of the integrated power spectral density with temperature shows that the mechanical mode equilibrates with the cryostat even for the lowest achievable temperature of 15 mK. This temperature corresponds to a thermal occupancy $n_m = 30$, where $n_m = [\exp(\hbar\Omega_m/k_B T) - 1]^{-1}$. The calibration determines the electromechanical coupling strength $G/2\pi = 49 \pm 2$ MHz/nm. With the device parameters, we can investigate both the fundamental sensitivity of our measurement as well as the effects of radiation pressure cooling.

The total measured displacement noise results from two sources: the membrane's actual mean-square motion S_x^{th} and the *apparent* motion S_x^{imp} due to imprecision of the measurement. Fig. 2a demonstrates how the use of low-noise parametric amplification significantly lowers S_x^{imp} , resulting in a reduction in the white-noise background by a factor of more than 30. This greatly increases the signal-to-noise ratio of the membrane's thermal motion, reducing the required integration time to resolve the thermal peak by a factor of 1000. To investigate the measurement sensitivity in the presence of dynamical backaction, we regulate the cryostat temperature at 20 mK and increase the amplitude of the detuned microwave drive while observing modifications in the displacement spectral density. We quantify the strength of the drive by the resulting number of photons n_d in the microwave cavity. As shown in Fig. 2b, the measurement imprecision S_x^{imp} is inversely proportional to n_d . At the highest drive power ($n_d \approx 10^5$), the absolute displacement sensitivity is 5.5×10^{-34} m²/Hz.

As expected, the increased drive power also damps and cools the mechanical oscillator [3, 23, 24]. The total mechanical dissipation rate Γ'_m is the sum of the intrinsic dissipation Γ_m and the radiation-pressure-induced damping resulting from scattering photons to the upper/lower sideband $\Gamma = \Gamma_+ - \Gamma_-$, where $\Gamma_{\pm} = 4g^2\kappa/[\kappa^2 + 4(\Delta \pm \Omega_m)^2]$. Here, g is the coupling rate between the cavity and the mechanical mode, which depends on the amplitude of the drive: $g = Gx_{z\text{p}}\sqrt{n_d}$. Fig. 2c shows the measured values of κ , g and Γ'_m as the drive increases. The radiation-pressure damping of the mechanical oscillator becomes pronounced above a cavity drive amplitude of approximately 75 photons, at which point $\Gamma = \Gamma_m$ and the mechanical linewidth has doubled.

While the absolute value of the displacement imprecision decreases with increasing power, the visibility of

the thermal mechanical peak no longer improves once the radiation-pressure force becomes the dominant dissipation mechanism for the membrane. By expressing the imprecision as equivalent thermal quanta of the oscillator $n_{\text{imp}} = \Gamma'_m S_x^{\text{imp}} / 8x_{\text{zp}}^2$, we see that the visibility of the thermal noise above the imprecision no longer improves once the drive is much greater than $n_d \approx 100$ (Fig. 2d). This is because a linear decrease in S_x^{imp} is balanced by a linear increase in Γ'_m due to radiation-pressure damping. The asymptotic value of n_{imp} is a direct measure of the efficiency of the microwave measurement. Ideally, for a lossless circuit, a quantum-limited microwave measurement would imply $n_{\text{imp}} = 1/4$. The incorporation of the low-noise JPA improves n_{imp} close to this ideal limit, reducing the asymptotic value of n_{imp} from 70 to 1.9 quanta. This level of sensitivity is crucial, as we will now use this measurement to resolve the residual thermal motion of the membrane as it is cooled into the quantum regime.

Beginning from a cryostat temperature of 20 mK and a thermal occupation of $n_m^T = 40$ quanta, the fundamental mechanical mode of the membrane is cooled by the radiation-pressure forces. Figure 3a shows the displacement spectral density of the motional sideband as n_d is increased from 18 to 4,500 photons along with fits to a Lorentzian lineshape (shaded area). As described above, this increased drive results in three effects on the spectra: lower noise floor, wider resonances and smaller area. As it is the area that corresponds to the mean-square motion of the membrane, it directly measures the effective temperature of the mode. At a drive intensity that corresponds to 4,000 photons in the cavity, the thermal occupation is reduced below one quantum of mechanical motion, entering the quantum regime.

Observing the noise spectrum over a broader frequency range reveals that there is also a second Lorentzian peak with linewidth κ whose area corresponds to the finite thermal occupation n_c of the cavity. Over a broad frequency range it is no longer valid to evaluate the cavity parameters at a single frequency to infer the spectrum in units of S_x . Instead, Fig. 3b shows the noise spectrum in units of sideband power normalized by the power at the drive frequency, S/P_o . These two sources of noise originating from either the mechanical or the electrical mode interfere with each other and result in noise squashing [13] and eventually normal-mode splitting [29] once $2g > \kappa/\sqrt{2}$. Using a quantum-mechanical description applied to our circuit [13, 25], the expected noise spectrum is

$$S/\hbar\omega = \frac{1}{2} + n_{\text{add}} + \frac{2\kappa_{\text{ex}} \left[\kappa n_c (\Gamma_m^2 + 4\delta^2) + 4\Gamma_m n_m^T g^2 \right]}{\left| 4g^2 + \left(\kappa + 2j(\delta + \tilde{\Delta}) \right) (\Gamma_m + 2j\delta) \right|^2} \quad (1)$$

where $\delta = \omega - \Omega_m$, $\tilde{\Delta} = \omega_d + \Omega_m - \omega_c$, and n_{add} is added noise of the microwave measurement expressed as an equivalent number of microwave photons. Fig. 3b shows the measured spectra and corresponding fits (shaded region) to Eq. 1 as the electromechanical system evolves

first into the quantum regime ($n_m, n_c < 1$) and then into the strong-coupling regime ($2g > \kappa/2$). The results are summarized in Fig. 3c, where the thermal occupancy of both the mechanical and electrical modes are shown as a function of n_d . For low drive power, the cavity shows no resolvable thermal population (to within our measurement uncertainty of 0.05 quanta) as expected for a 7.5 GHz mode at 20 mK. While it is unclear whether the observed population at higher drive power is a consequence of direct heating of the substrate, heating of the microwave attenuators preceding the circuit, or intrinsic cavity frequency noise, we have determined that it is not the result of frequency or amplitude noise of our microwave generator, as this noise is reduced far below the microwave shot-noise level with narrow-band filtering and cryogenic attenuation (see Supplementary Information). Sideband cooling can never reduce the occupancy of the mechanical mode below that of the cavity. Therefore, in order for the system to access the quantum regime, the thermal population of the cavity must remain less than one quantum. Assuming $\Omega_m \gg \kappa$, the final occupancy of a mechanical mode is [29]

$$n_m = n_m^T \left(\frac{\Gamma_m}{\kappa} \frac{4g^2 + \kappa^2}{4g^2 + \kappa\Gamma_m} \right) + n_c \left(\frac{4g^2}{4g^2 + \kappa\Gamma_m} \right). \quad (2)$$

This equation shows that for moderate coupling ($\sqrt{\kappa\Gamma_m} \ll g \ll \kappa$) the cooling of the mechanical mode is linear in the number of drive photons. Beyond this regime, the onset of normal-mode splitting abates further cooling. Here the mechanical cooling rate becomes limited not by the coupling between the mechanical mode and the cavity, but instead by the coupling rate κ between the cavity and its environment [29]. Thus, the final occupancy of the mechanical mode can never be reduced to lower than $n_m^T \Gamma_m / \kappa$, and a stronger parametric drive will only increase the rate at which the thermal excitations Rabi oscillate between the cavity and mechanical modes. For our device we achieve the desired hierarchy: as the coupling is increased, we first cool to the ground state and then enter the strong-coupling regime ($n_m^T \Gamma_m < \kappa < g$). Once n_d exceeds 2×10^4 , the mechanical occupancy converges toward the cavity population, reaching a minimum of 0.34 ± 0.05 quanta. At the highest power drive power ($n_d = 2 \times 10^5$) the mechanical mode has hybridized with the cavity, resulting in the normal-mode splitting characteristic of the strong-coupling regime [16]. This level of coupling is required to utilize the hybrid system for quantum information processing, as it is only in the strong-coupling regime that a quantum state may be manipulated faster than it decoheres from the coupling of either the electromagnetic or mechanical modes to the environment.

Together the measurements shown in Fig. 2 and 3 quantify the overall measurement efficiency of the system. The Heisenberg limit requires that a continuous displacement measurement is necessarily accompanied by a backaction force [3, 12, 25], such that $\sqrt{S_x^{\text{imp}} S_F} \geq \hbar$, where S_F is the force noise spectral density. From the thermal occupancy

and damping rate of the mechanical mode, we extract the total force spectral density $S_F = 4\hbar\Omega_m m\Gamma'_m(n_m + 1/2)$. This places a conservative upper bound on the quantum backaction by assuming that it alone is responsible for the finite occupancy of the mechanical mode. This experiment achieves the closest approach to Heisenberg-limited displacement detection to date [14, 25] with a lowest imprecision-backaction product $\sqrt{S_x^{\text{imp}}S_F} = 4\hbar\sqrt{n_{\text{imp}}(n_m + 1/2)} = (5.1 \pm 0.4)\hbar$. Thus, this mechanical device simultaneously demonstrates ground-state preparation, strong-coupling and near quantum-limited detection.

Looking forward, this technology offers a feasible route to achieve many of the longstanding goals for quantum *mechanical* systems. These prospects include a direct measurement of the zero-point motion, observation of the fundamental asymmetry between the rate of emission and absorption of phonons [1], quantum nondemolition measurements [3] and generation of entangled states of mechanical motion [17, 18]. Furthermore, combining this device with a single-photon source and detector (such as a superconducting qubit [22, 30]) would enable preparation of arbitrary quantum states of mechanical motion as well as observation of a single excitation as it Rabi oscillates between a 7 GHz photon and a 10 MHz phonon [20]. Because the interaction between the mechanical mode and the cavity is parametric, the coupling strength is inherently tunable and can be turned on and off quickly. Thus, once a quantum state is transferred into the mechanical mode, it can be stored there for a time $\tau_{\text{th}} = 1/(n_m^T\Gamma_m) > 100 \mu\text{s}$ before absorbing one thermal phonon from its environment. As this timescale is much longer than typical coherence times of superconducting qubits, mechanical modes offer the potential for delay and storage of quantum information. Lastly, because mechanical oscillators can couple to light of any frequency, they could serve as a unique intermediary that transfers quantum information between the microwave and optical domains [21].

These measurements demonstrate the power of sideband techniques to cool a macroscopic ($\sim 10^{12}$ atoms) mechanical mode, beyond what is feasible with conventional refrigeration techniques, into the quantum regime. These broadly applicable methods for state preparation, manipulation and detection, pave the way to access the quantum nature of a wide class of long-lived mechanical oscillators. Through the strong interaction between photons and phonons, mechanical systems can now inherit the experimental and theoretical power of quantum optics, opening the field of quantum acoustics.

ACKNOWLEDGEMENTS

We thank A. W. Sanders for taking the micrograph in Fig. 1a and thank the JILA instrument shop for fabrication

and design of the cavity filter. This work was financially supported by NIST and the DARPA QuASAR program. T.D. acknowledges support from the Deutsche Forschungsgemeinschaft (DFG). Contribution of the U.S. government, not subject to copyright.

AUTHOR INFORMATION

Reprints and permissions information is available at www.nature.com/reprints. The authors declare no competing financial interests. Correspondence and requests for materials should be addressed to J.D.T (john.teufel@nist.gov).

-
- [1] Diedrich, F., Bergquist, J. C., Itano, W. M. & Wineland, D. J. Laser cooling to the zero-point energy of motion. *Phys. Rev. Lett.* **62**, 403–406 (1989).
 - [2] Anderson, M. H., Ensher, J. R., Matthews, M. R., Wieman, C. E. & Cornell, E. A. Observation of bose-einstein condensation in a dilute atomic vapor. *Science* **269**, 198–201 (1995).
 - [3] Braginsky, V. B. & Khalili, F. Y. *Quantum Measurement* (Cambridge University Press, 1992).
 - [4] Kippenberg, T. J. & Vahala, K. J. Cavity optomechanics: Back-action at the mesoscale. *Science* **321**, 1172–1176 (2008).
 - [5] Braginsky, V. B., Manukin, A. B. & Tikhonov, M. Y. Investigation of dissipative ponderomotive effects of electromagnetic radiation. *Sov. Phys. JETP* **31**, 829 (1970).
 - [6] Blair, D. G. *et al.* High sensitivity gravitational wave antenna with parametric transducer readout. *Phys. Rev. Lett.* **74**, 1908–1911 (1995).
 - [7] Teufel, J. D., Harlow, J. W., Regal, C. A. & Lehnert, K. W. Dynamical backaction of microwave fields on a nanomechanical oscillator. *Phys. Rev. Lett.* **101**, 197203 (2008).
 - [8] Thompson, J. D. *et al.* Strong dispersive coupling of a high-finesse cavity to a micromechanical membrane. *Nature* **452**, 72–75 (2008).
 - [9] Gröblacher, S. *et al.* Demonstration of an ultracold micro-optomechanical oscillator in a cryogenic cavity. *Nature Physics* **5**, 485–488 (2009).
 - [10] Park, Y.-S. & Wang, H. Resolved-sideband and cryogenic cooling of an optomechanical resonator. *Nature Physics* **5**, 489–493 (2009).
 - [11] Lin, Q., Rosenberg, J., Jiang, X., Vahala, K. J. & Painter, O. Mechanical oscillation and cooling actuated by the optical gradient force. *Phys. Rev. Lett.* **103**, 103601 (2009).
 - [12] Schliesser, A., Arcizet, O., Riviere, R., Anetsberger, G. & Kippenberg, T. J. Resolved-sideband cooling and position measurement of a micromechanical oscillator close to the Heisenberg uncertainty limit. *Nature Physics* **5**, 509–514 (2009).
 - [13] Rocheleau, T. *et al.* Preparation and detection of a mechanical resonator near the ground state of motion. *Nature* **463**, 72–75 (2010).

- [14] Rivière, R. *et al.* Optomechanical sideband cooling of a micromechanical oscillator close to the quantum ground state. *arXiv:1011.0290* (2010).
- [15] Li, T., Kheifets, S. & Raizen, M. G. Millikelvin cooling of an optically trapped microsphere in vacuum. *arXiv:1101.1283* (2011).
- [16] Teufel, J. D. *et al.* Circuit cavity electromechanics in the strong-coupling regime. *Nature* **471**, 204–208 (2011).
- [17] Bose, S., Jacobs, K. & Knight, P. L. Preparation of nonclassical states in cavities with a moving mirror. *Phys. Rev. A* **56**, 4175 (1997).
- [18] Mancini, S., Man’ko, V. I. & Tombesi, P. Ponderomotive control of quantum macroscopic coherence. *Phys. Rev. A* **55**, 3042 (1997).
- [19] Marshall, W., Simon, C., Penrose, R. & Bouwmeester, D. Towards quantum superpositions of a mirror. *Phys. Rev. Lett.* **91**, 130401 (2003).
- [20] Akram, U., Kiesel, N., Aspelmeyer, M. & Milburn, G. J. Single-photon opto-mechanics in the strong coupling regime. *New Journal of Physics* **12**, 083030 (2010).
- [21] Regal, C. A. & Lehnert, K. W. From cavity electromechanics to cavity optomechanics. *Journal of Physics: Conference Series* **264**, 012025 (2011).
- [22] O’Connell, A. D. *et al.* Quantum ground state and single-phonon control of a mechanical resonator. *Nature* **464**, 697–703 (2010).
- [23] Marquardt, F., Chen, J. P., Clerk, A. A. & Girvin, S. M. Quantum theory of cavity-assisted sideband cooling of mechanical motion. *Phys. Rev. Lett.* **99**, 093902 (2007).
- [24] Wilson-Rae, I., Nooshi, N., Zwerger, W. & Kippenberg, T. J. Theory of ground state cooling of a mechanical oscillator using dynamical backaction. *Phys. Rev. Lett.* **99**, 093901 (2007).
- [25] Clerk, A. A., Devoret, M. H., Girvin, S. M., Marquardt, F. & Schoelkopf, R. J. Introduction to quantum noise, measurement, and amplification. *Rev. Mod. Phys.* **82**, 1155–1208 (2010).
- [26] Cicak, K. *et al.* Low-loss superconducting resonant circuits using vacuum-gap-based microwave components. *Appl. Phys. Lett.* **96**, 093502 (2010).
- [27] Castellanos-Beltran, M. A., Irwin, K. D., Hilton, G. C., Vale, L. R. & Lehnert, K. W. Amplification and squeezing of quantum noise with a tunable Josephson metamaterial. *Nature Physics* **4**, 929–931 (2008).
- [28] Teufel, J. D., Donner, T., Castellanos-Beltran, M. A., Harlow, J. W. & Lehnert, K. W. Nanomechanical motion measured with an imprecision below that at the standard quantum limit. *Nature Nanotechnology* **4**, 820–823 (2009).
- [29] Dobrindt, J. M., Wilson-Rae, I. & Kippenberg, T. J. Parametric normal-mode splitting in cavity optomechanics. *Phys. Rev. Lett.* **101**, 263602 (2008).
- [30] Hofheinz, M. *et al.* Synthesizing arbitrary quantum states in a superconducting resonator. *Nature* **459**, 546–549 (2009).

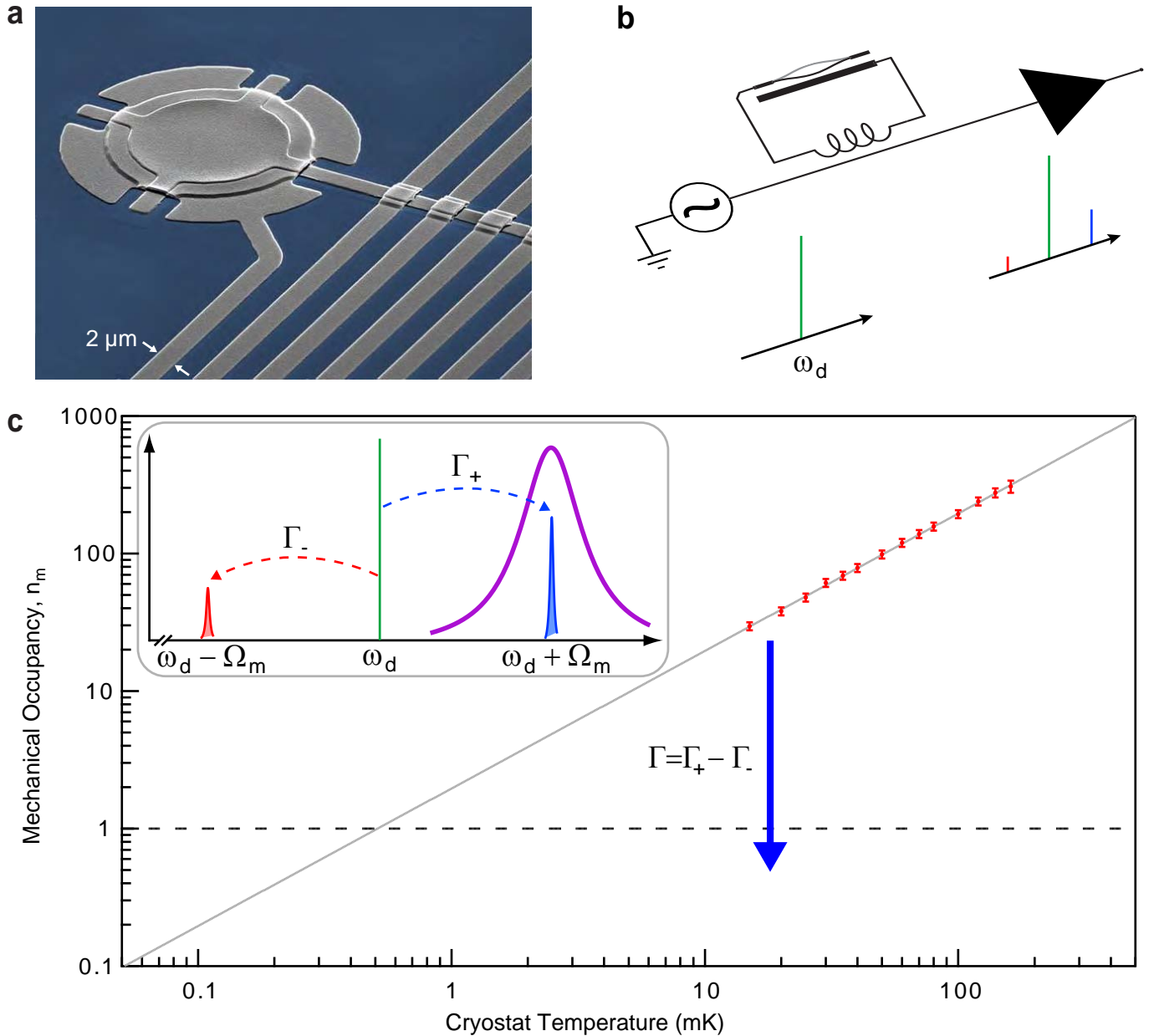


FIG. 1. **Schematic description of the experiment.** **a**, Colorized scanning electron micrograph showing the aluminum (grey) electromechanical circuit fabricated on a sapphire (blue) substrate, in which a 15 μm diameter membrane is lithographically suspended 50 nm above a lower electrode. The membrane's motion modulates the capacitance, and hence, the resonance frequency of the superconducting microwave circuit. **b**, A coherent microwave drive inductively coupled to the circuit acquires modulation sidebands due to the thermal motion of the membrane. The upper sideband is amplified with a nearly quantum-limited Josephson parametric amplifier within the cryostat. **c**, The microwave power in the upper sideband provides a direct measurement of the thermal occupancy of the mechanical mode, which may be calibrated *in situ* by varying the temperature of the cryostat. The mechanical mode shows thermalization with the cryostat at all temperatures, yielding a minimum thermal occupancy of 30 mechanical quanta without employing sideband-cooling techniques. The inset illustrates the concept of sideband cooling. When the circuit is excited with a detuned microwave drive such that $\Delta = -\Omega_m$, the narrow line shape of the electrical resonance ensures that photons are preferentially scattered to higher energy, providing a cooling mechanism for the membrane.

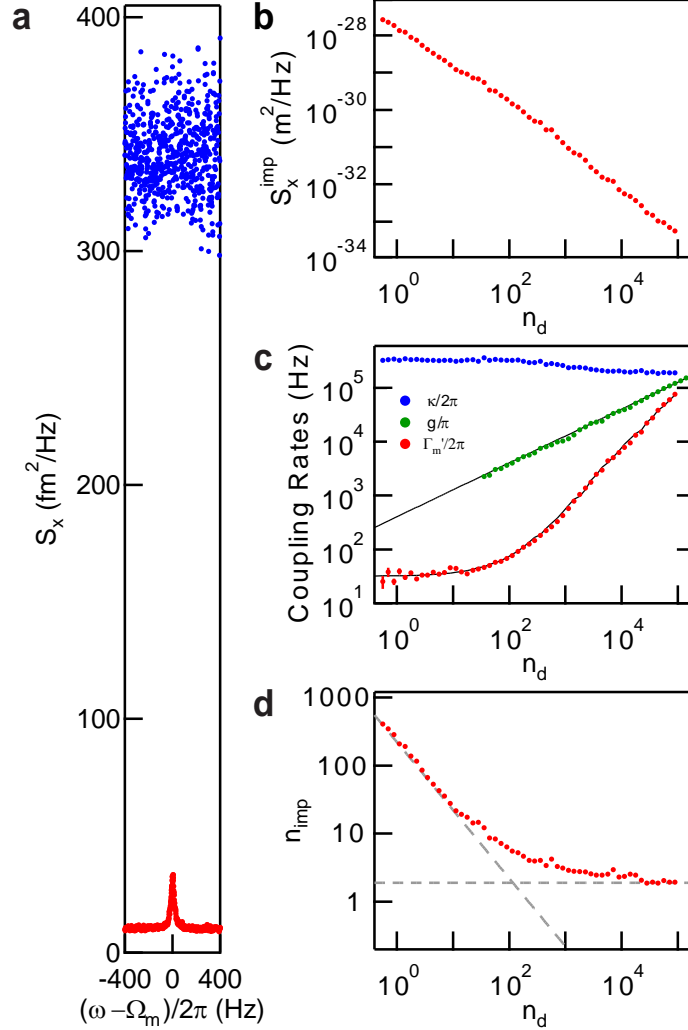


FIG. 2. Displacement sensitivity in the presence of radiation-pressure damping. **a**, The displacement spectral density measured with (red) and without (blue) the Josephson parametric amplifier. As the parametric amplifier greatly reduces the total noise of the microwave measurement, the time required to resolve the thermal motion is reduced by a factor of 1000. **b**, As the microwave drive power is increased, the absolute displacement sensitivity, S_x^{imp} improves, reaching a minimum of $5.5 \times 10^{-34} \text{ m}^2/\text{Hz}$ at the highest power. **c**, The parametric coupling g between the microwave cavity and the mechanical mode increases as $\sqrt{n_d}$. This coupling damps the mechanical mode from its intrinsic linewidth of $\Gamma_m = 2\pi \times 32 \text{ Hz}$ until it is increased to that of the microwave cavity κ . **d**, The relative measurement imprecision, in units of mechanical quanta, depends on the product of S_x^{imp} and Γ'_m . Thus, once the power is large enough that radiation-pressure damping overwhelms the intrinsic mechanical dissipation, n_{imp} asymptotically approaches a constant value ($n_{\text{imp}} = 1.9$), which is a direct measure of the overall efficiency of the photon measurement.

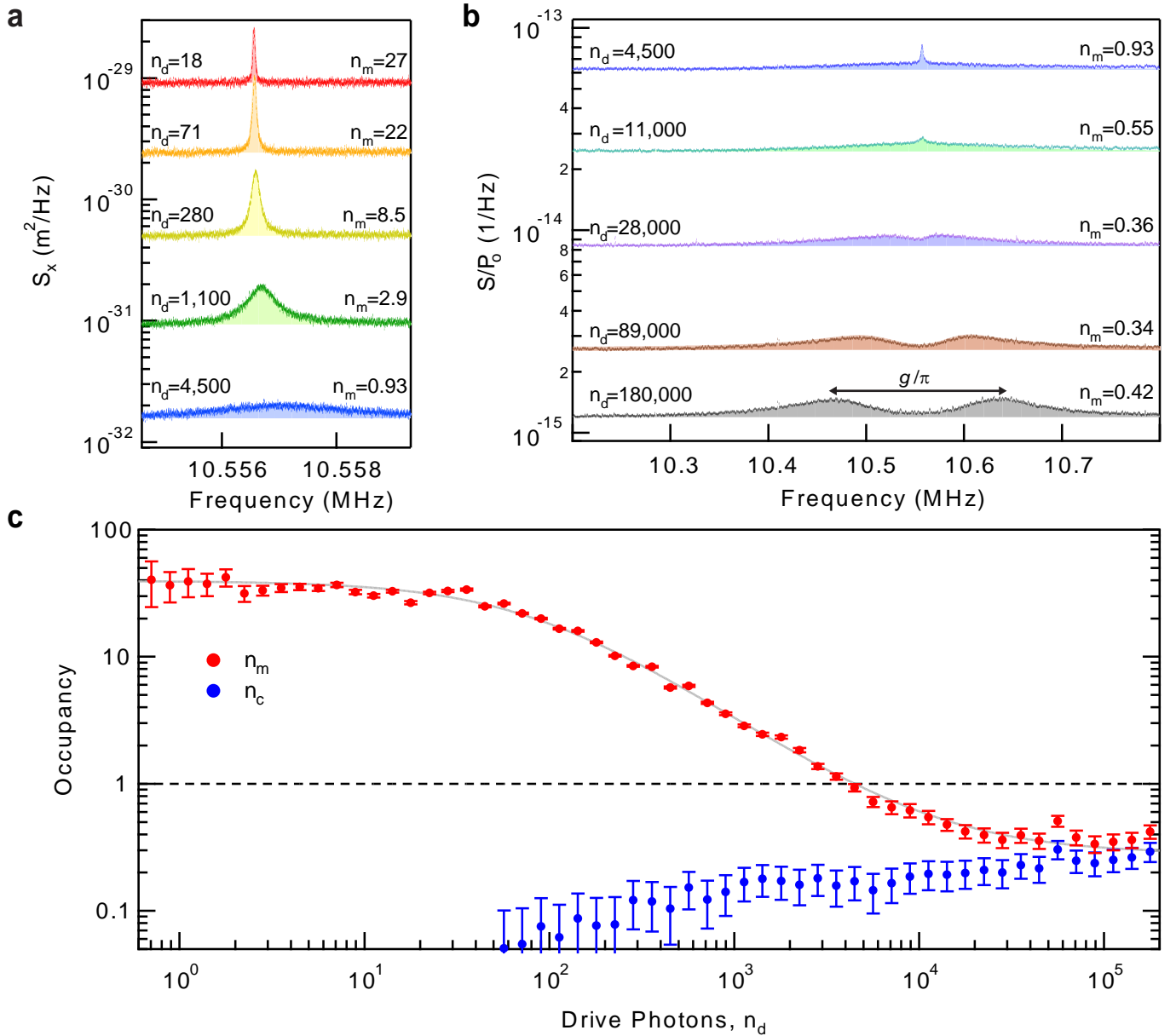


FIG. 3. Sideband cooling the mechanical mode to the ground state. **a**, The displacement noise spectra and Lorentzian fits (shaded region) for five different drive powers. With higher power, the mechanical mode is both damped (larger linewidth) and cooled (smaller area) by the radiation pressure forces. **b**, Over a broader frequency span, the normalized sideband noise spectra clearly show both the narrow mechanical peak and a broader cavity peak due to finite occupancy of the mechanical and electrical modes, respectively. A small, but resolvable, thermal population of the cavity appears as the drive power increases, setting the limit for the final occupancy of the coupled optomechanical system. At the highest drive power, the coupling rate between the mechanical oscillator and the microwave cavity exceeds the intrinsic dissipation of either mode, and the system hybridizes into optomechanical normal modes. **c**, Starting in thermal equilibrium with the cryostat at $T = 20$ mK, sideband cooling reduces the thermal occupancy of the mechanical mode from $n_m = 40$ into the quantum regime, reaching a minimum of $n_m = 0.34 \pm 0.05$. These data demonstrate that the parametric interaction between photons and phonons can initialize the strongly coupled, electromechanical system in its quantum ground state.

Supplementary Information for “Sideband Cooling Micromechanical Motion to the Quantum Ground State”

NOISE SPECTRUM OF AN OPTOMECHANICAL SYSTEM

A mechanical degree of freedom that parametrically couples to the cavity resonance frequency modifies the power emerging from the cavity by scattering photons to the upper or lower mechanical sidebands. To calculate the full noise spectrum of the optomechanical system, we follow the general method of input-output theory [1]. We define $g = Gx_{zp}\sqrt{n_d}$, where $G = d\omega_c/dx$, $x_{zp} = \sqrt{\hbar/2m\Omega_m}$, m is the mass, ω_c is the cavity resonance frequency, Ω_m is the mechanical resonance frequency and n_d is the number of photons in the cavity due to a drive at frequency ω_d . Furthermore, we define the response functions of the mechanical and cavity modes as $\chi_c^{-1} = \kappa/2 + j(\delta + \tilde{\Delta})$ and $\chi_m^{-1} = \Gamma_m/2 + j\delta$, where Γ_m is the mechanical dissipation rate, κ is the cavity dissipation rate, $\delta = \omega - \Omega_m$, $\tilde{\Delta} = \omega_d - \omega_c + \Omega_m$ and $j = \sqrt{-1}$. κ is total cavity dissipation rate due to both the intentional coupling to the transmission line κ_{ex} and the intrinsic losses κ_0 . From these parameters, we define the optomechanical self-energy [2, 3] as a function of δ :

$$\Sigma(\delta) = -jg^2 [\chi_c(\delta) - \chi_c^*(\delta + 2\Omega_m)] \quad (\text{S1})$$

$$\approx -jg^2 \chi_c(\delta) \quad (\text{S2})$$

The approximation assumes that the drive is near the optimal detuning for cooling ($|\tilde{\Delta}| \ll \Omega_m$) and the system is sufficiently in the good-cavity limit ($\Omega_m \gg \kappa$) such that the cavity response at $(\delta + 2\Omega_m)$ may be neglected. Now the effective mechanical response function $\tilde{\chi}_m$ including the optomechanical effects is:

$$\tilde{\chi}_m = \frac{\chi_m}{1 + j\chi_m \Sigma} \quad (\text{S3})$$

$$\approx \frac{\chi_c^{-1}}{g^2 + \chi_m^{-1} \chi_c^{-1}} \quad (\text{S4})$$

The noise at the output of the cavity is characterized by the noise operator \hat{b}_{out} , which is related to the cavity field operator \hat{a} by $\hat{b}_{\text{out}} = \sqrt{\beta\kappa_{\text{ex}}}\hat{a}$. β is a dimensionless factor that depends on the geometry. Our circuit (shown schematically in Fig. S1) couples power from the cavity equally to the output and back to the input so here $\beta = 1/2$. In principle, this fraction could be engineered by coupling asymmetrically to the input and the output, or by using a single port cavity ($\beta = 1$). Following directly the theoretical analysis of previous work [3, 4], we consider the noise operators $\hat{\eta}_m$ and $\hat{\eta}_c$ associated with the mechanical and cavity modes respectively, which satisfy the relations

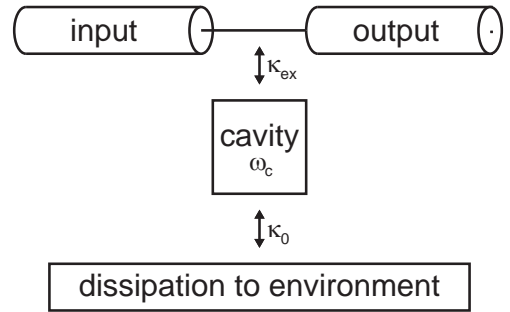


FIG. S1. Cavity coupling block diagram.

$\langle \hat{\eta}_m^\dagger \hat{\eta}_m \rangle = n_m^T$ and $\langle \hat{\eta}_c^\dagger \hat{\eta}_c \rangle = n_c$. Thus, the output noise is [4]

$$\begin{aligned} \hat{b}_{\text{out}} = & -\sqrt{\beta\kappa_{\text{ex}}}\chi_c\sqrt{\kappa}(1 - g^2\tilde{\chi}_m\chi_c)\hat{\eta}_c \\ & -\sqrt{\beta\kappa_{\text{ex}}}\chi_c\sqrt{\Gamma_m}(jg\tilde{\chi}_m)\hat{\eta}_m. \end{aligned}$$

In the frequency domain, the power spectral density of the noise at the output (in units of W/Hz) is $S = \hbar\omega \langle \hat{b}_{\text{out}}^\dagger \hat{b}_{\text{out}} \rangle$,

$$\begin{aligned} S = & \frac{4\hbar\omega\beta\kappa_{\text{ex}}(\Gamma_m^2 + 4\delta^2)\kappa n_c}{\left|4g^2 + (\kappa + 2j(\delta + \tilde{\Delta}))(\Gamma_m + 2j\delta)\right|^2} \\ & + \frac{16\hbar\omega\beta\kappa_{\text{ex}}g^2\Gamma_m n_m^T}{\left|4g^2 + (\kappa + 2j(\delta + \tilde{\Delta}))(\Gamma_m + 2j\delta)\right|^2}. \end{aligned}$$

The first term simply represents the thermal noise of a cavity with occupancy n_c whose spectral weight is distributed over the ‘dressed’ cavity mode. The ‘dressed’ cavity mode includes the effect of optomechanically induced transparency [7? ?] and reduces to a single Lorentzian lineshape in the limit of weak coupling ($g \ll \sqrt{\kappa\Gamma_m}$). The second term is the thermal noise of the mechanical mode with its modified mechanical susceptibility. Unlike previous derivations [4], we have not assumed the weak-coupling regime. Thus, as this equation is valid in both the weak- and strong-coupling regimes, it gives a unified description of the thermal noise spectrum even in the presence of normal-mode splitting. Finally, the total noise at the output of the measurement including the vacuum noise of the photon field and the added noise of the measurement is

$$\frac{S}{\hbar\omega} = \frac{1}{2} + n'_{\text{add}} + \frac{4\beta\kappa_{\text{ex}}[\kappa n_c(\Gamma_m^2 + 4\delta^2) + 4\Gamma_m n_m^T g^2]}{\left|4g^2 + (\kappa + 2j(\delta + \tilde{\Delta}))(\Gamma_m + 2j\delta)\right|^2}, \quad (\text{S5})$$

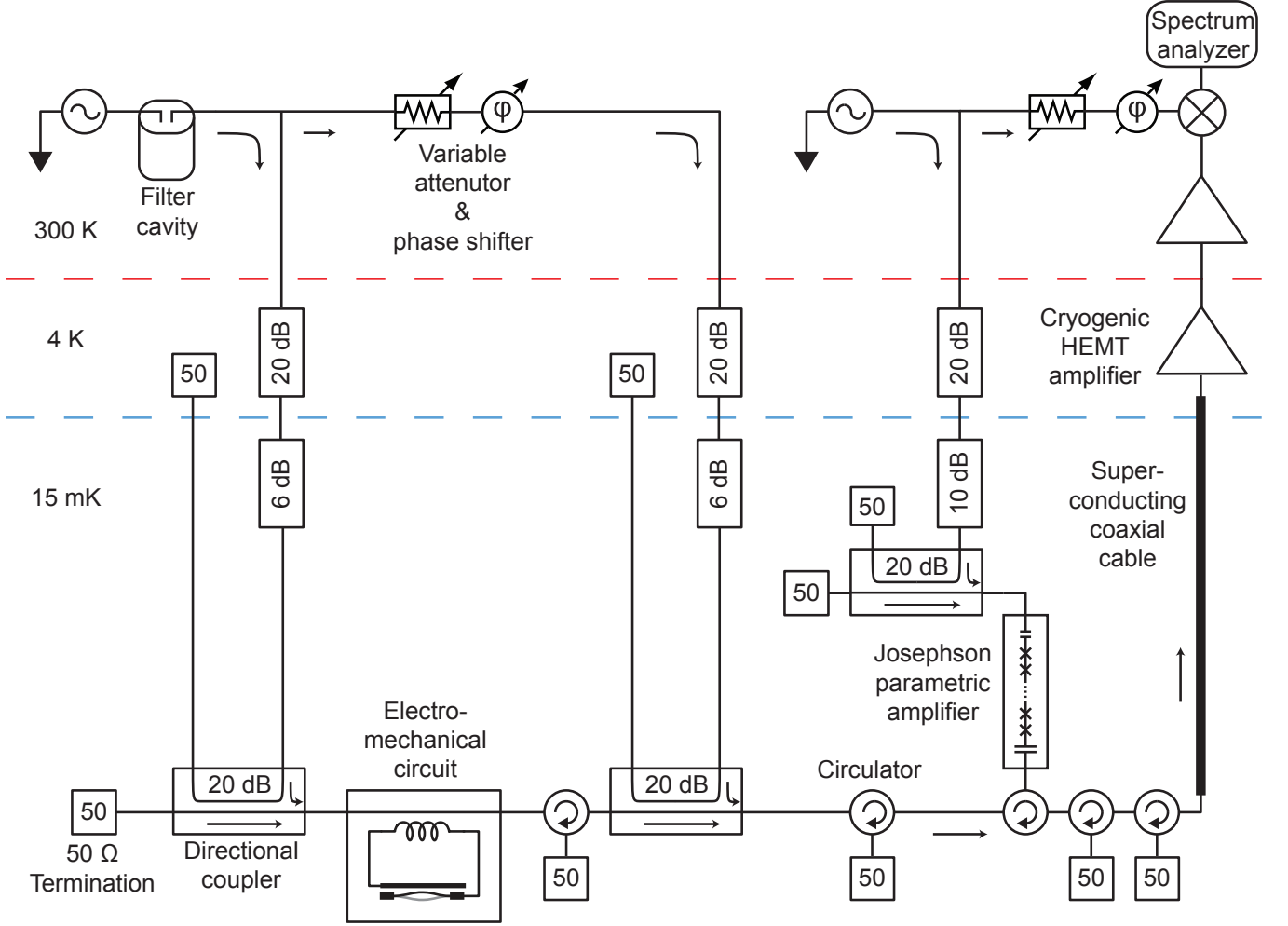


FIG. S2. **Detailed schematic diagram.** A microwave generator creates a tone at the drive frequency. This signal is filtered with a resonant cavity at room temperature and split into two arms. The first arm excites the cavity through approximately 53 dB of cryogenic attenuation. In order to avoid saturating the low-noise amplifier with the microwave drive tone, the second arm is used to cancel the drive before amplification. A computer-controlled variable attenuator and phase shifter are run in a feedback loop to maintain cancellation at the part per million level. A second microwave generator is used to provide the pump tone for the Josephson parametric amplifier (JPA) as well as the reference oscillator for the mixer. This pump tone is 1.3 MHz above ω_c so that the JPA is operated as a non-degenerate parametric amplifier, which measures both quadratures of the electromagnetic field at the upper sideband frequency. The last stage of attenuation on all lines occurs inside a 20 dB directional coupler, which allows us to minimize the microwave power dissipated on the cold stage of the cryostat. The JPA is a reflection amplifier; a signal incident on the strongly coupled port of the JPA is reflected and amplified. A cryogenic circulator is used to separate the incident and reflected waves, defining the input and output ports of the JPA. The other circulators are used to isolate the cavity from the noise emitted from the amplifier's input.

where n'_{add} is the total added noise of the measurement in units of equivalent number of photons. For an ideal measurement (*i.e.* for a quantum-limited measurement of both quadratures of the light field), $n'_{\text{add}} = 1/2$.

Before the onset of normal-mode splitting, one can directly relate the measured microwave power spectrum S to the displacement spectral density S_x . Assuming $\tilde{\Delta} = 0$,

$$n_c \ll n_m \text{ and } g, \delta \ll \kappa,$$

$$\frac{S}{\hbar\omega} = \frac{1}{2} + n'_{\text{add}} + 4\beta \frac{\kappa_{\text{ex}}}{\kappa} \Gamma \frac{\Gamma_m n_m^T}{(\Gamma_m + \Gamma)^2 + 4\delta^2} \quad (\text{S6})$$

$$= \frac{1}{2} + n'_{\text{add}} + \frac{2\beta G^2 n_d}{\kappa} \frac{\kappa_{\text{ex}}}{\kappa} S_x, \quad (\text{S7})$$

where $\Gamma = 4g^2/\kappa$ is the optomechanical damping rate.

MICROWAVE MEASUREMENT AND CALIBRATION

The detailed circuit diagram for our measurements is shown in Fig. S2. In order to calibrate the value of $g_0 = Gx_{zp}$ for this device, we applied a microwave drive optimally red-detuned ($\tilde{\Delta} = 0$) and measured the thermal noise spectrum of the mechanical oscillator as a function of cryostat temperature. Here we restricted $n_d \approx 3$ in order to ensure that radiation pressure effects are negligible. With the value of g_0 now determined, we increase the drive amplitude and measure the thermal noise spectrum at each drive power. The noise spectra are recorded and averaged with commercial FFT spectrum analyser. Each spectrum is typically an average of 500 traces with a measurement time of 0.5 s per trace. The cavity response is then measured with a weak probe tone with a vector network analyser to determine precise cavity parameters at each microwave drive power, including the precise detuning and κ . For larger microwave drive powers where the cavity spectrum exhibits optomechanically induced transparency effects [7? ?], this spectrum also serves as a direct measure of g . Finally, using additional calibration tones, each noise spectrum is calibrated in units of absolute microwave noise quanta and fit with Eq. 5 to determine the occupancy of both the cavity and mechanical modes.

For our measurements, we infer that our entire measurement chain has an effective added noise of $n'_{\text{add}} = 2.1$. This value is consistent with the independently measured value for the added noise of the JPA ($n_{\text{add}} = 0.8$) and the 2.5 dB of loss between the output of the cavity and the JPA [8, 9].

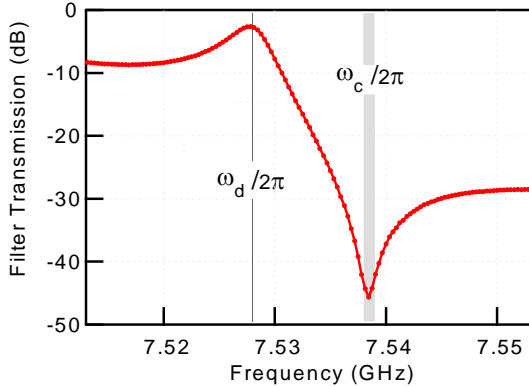


FIG. S3. **Measured transmission of filter cavity.** A tunable resonant cavity was implemented at room temperature in order to suppress noise ~ 10 MHz above the drive frequency. As shown here, this cavity reduces the noise at the cavity frequency by more than 40 dB, ensuring that the phase or amplitude noise of the generator is not responsible for the finite occupancy of the cavity at large drive power.

In order to ensure that the amplitude or phase noise of the signal generator was not responsible for the finite occupancy of the cavity at high drive power, we designed and

built a custom filter cavity [4]. As shown in Fig. S3, when the filter cavity is tuned to precisely the frequencies of our circuit, it provides an addition 40 dB of noise suppression at the cavity resonance frequency. The phase and amplitude noise of our signal generator alone are specified by the manufacturer to be less than -150 dBc at Fourier frequencies 10 MHz away from the drive. With the addition of filter cavity, we lower this noise to well below the shot-noise level of our microwave drive. Furthermore, even without the filter cavity, we could not resolve an appreciable difference in the cavity occupancy. Thus, while we do not know the precise mechanism for this occupancy, we conclusively determine the generator noise is not the cause.

INFERRING CAVITY PARAMETER AND NUMBER OF DRIVE PHOTONS

The measured microwave cavity parameters may be inferred from the transmitted power spectrum. The power at the output of the cavity P_o is related to the input power P_i by [7]

$$P_o = P_i \left(\frac{\kappa_0^2 + 4\Delta^2}{\kappa^2 + 4\Delta^2} \right), \quad (\text{S8})$$

where $\Delta = \omega_d - \omega_c$ is the difference between the frequency of the drive ω_d and the cavity resonance frequency ω_c . κ is the total intensity decay rate of the cavity (full width at half maximum) with $\kappa = \kappa_0 + \kappa_{\text{ex}}$. κ_0 is the coupling rate to the dissipative environment, and κ_{ex} is the coupling rate to the transmission line used to excite and monitor the cavity.

The number of photons in the cavity due to a coherent input drive at detuning Δ may be calculated from the stored energy E in the cavity.

$$n_d = \frac{E}{\hbar\omega_d} = \frac{2P_i}{\hbar\omega_d} \frac{\kappa_{\text{ex}}}{\kappa^2 + 4\Delta^2} \quad (\text{S9})$$

For our circuit, $\kappa_{\text{ex}} = 2\pi \times 133$ kHz. Thus, when the drive is optimally detuned such that $\Delta = -\Omega_m$, the input power required to excite the cavity with one photon is $P_i \approx 2\hbar\omega_d\Omega_m^2/\kappa_{\text{ex}} \approx 50$ fW.

FUNDAMENTAL LIMITS OF SIDEBAND COOLING

Equation 2 in the main text gives an expression for the final occupancy of a mechanical mode, assuming that the microwave drive is optimally detuned ($\Delta = -\Omega_m$). This expression is only the lowest order approximation in the small quantities g/Ω_m and κ/Ω_m . Up to second order, the

final occupancy is [10]

$$n_m = n_m^T \left(\frac{\Gamma_m}{\kappa} \frac{4g^2 + \kappa^2}{4g^2 + \kappa\Gamma_m} \right) \left[1 + \frac{g^2}{\Omega_m^2} \frac{4g^2 + \kappa\Gamma_m}{4g^2 + \kappa^2} \right] + n_c \left(\frac{4g^2}{4g^2 + \kappa\Gamma_m} \right) \left[1 + \frac{8g^2 + \kappa^2}{8\Omega_m^2} \frac{4g^2 + \kappa\Gamma_m}{4g^2} \right] + \frac{8g^2 + \kappa^2}{16\Omega_m^2}.$$

The last term represents the fundamental limit for sideband cooling and demonstrates the importance of the resolved-sideband regime. For our system, $\Omega_m \gg \kappa, g$; and hence this last term only contributes negligibly to the final occupancy of the mechanical mode ($< 10^{-4}$ quanta).

Measurement imprecision and backaction

Throughout the main text and this supplementary information, we use the “single-sided” convention for all spectral densities in which for any quantity A , the mean-square fluctuations are $\langle A^2 \rangle = \int_0^\infty S_A(\omega) \frac{d\omega}{2\pi}$. This yields the familiar classical result that an oscillator coupled to a thermal bath of temperature T will experience a random force characterized by the force spectral density $S_F = 4k_B T m \Gamma_m$. More generally,

$$S_F = 4\hbar\Omega_m \left(n_m^T + \frac{1}{2} \right) m \Gamma_m, \quad (\text{S10})$$

where n_m^T is the Bose-Einstein occupancy factor given by $n_m^T = [\exp(\hbar\Omega_m/k_B T) - 1]^{-1}$.

Independent of any convention for defining the spectral density, the visibility of a thermal mechanical peak of given mechanical occupancy above the noise floor of the measurement represents a direct measure of the overall efficiency of the detection. As shown in Fig. S4, ratio of the peak height to the white-noise background allows us to quantify the imprecision of the measurement in units of mechanical quanta [9], $n_{\text{imp}} \equiv S_x^{\text{imp}} m \Omega_m \Gamma_m / (4\hbar)$. Inspection of Eq. S6 implies

$$n_{\text{imp}} = \frac{1}{4\beta} \frac{\kappa}{\kappa_{\text{ex}}} \frac{4g^2 + \kappa\Gamma_m}{4g^2} \left(\frac{1}{2} + n'_{\text{add}} \right) \quad (\text{S11})$$

Once the drive is strong enough that $g \gg \sqrt{\kappa\Gamma_m}$, n_{imp} no longer decreases with increasing drive. It is precisely because we are measuring with a detuned drive that also damps the mechanical motion, that n_{imp} asymptotically approaches a constant value [3, 11]. For an ideal measurement ($\beta = 1$, $\kappa = \kappa_{\text{ex}}$, and $n'_{\text{add}} = 1/2$), $n_{\text{imp}} \rightarrow 1/4$. Implicit in obtaining this optimal value for n'_{add} and hence n_{imp} is that all the photons exiting the cavity are measured. Any losses between the cavity and the detector can be modeled as a beam-splitter that only transmits a fraction η of the

photons to the detector and adds a fraction $(1 - \eta)$ of vacuum noise. So the effective added noise n'_{add} accounting for these losses becomes

$$n'_{\text{add}} = \frac{n_{\text{add}}}{\eta} + \left(\frac{1 - \eta}{\eta} \right) \frac{1}{2}, \quad (\text{S12})$$

Thus, shot-noise limited detection of the photons ($n_{\text{add}} = 1/2$) is a necessary, but not sufficient, condition for reaching the best possible level of precision.

Quantum mechanics also requires that a continuous displacement measurement must necessarily impart a force back on the measured object. For an optimally detuned drive ($\tilde{\Delta} = 0$) in the resolved-sideband regime, this backaction force spectral density S_F^{ba} approaches a constant value as a function of increasing drive strength and asymptotically approaches $S_F^{\text{ba}} = 2\hbar\Omega_m m \Gamma_m'$. Again, expressing the spectral density in units of mechanical quanta gives $n_{\text{ba}} \equiv S_F^{\text{ba}} / (4\hbar\Omega_m m \Gamma_m') \rightarrow 1/2$.

Fundamentally, the Heisenberg limit does not restrict the imprecision S_x^{imp} or the backaction S_F^{ba} alone, but rather it requires their product has a minimum value [3, 12]

$$\sqrt{S_x^{\text{imp}} S_F^{\text{ba}}} = 4\hbar\sqrt{n_{\text{imp}} n_{\text{ba}}} \geq \hbar. \quad (\text{S13})$$

An ideal cavity optomechanical system can achieve this lower limit for a continuous measurement with a drive applied at the cavity resonance frequency. When considering the case where the drive is instead applied detuned below the cavity resonance ($\tilde{\Delta} = 0$), this product never reaches this lower limit [3, 11] and is at minimum $\sqrt{S_x^{\text{imp}} S_F^{\text{ba}}} = \hbar\sqrt{2}$.

To estimate these quantities for our measurements, we can infer the total force spectral density experienced by

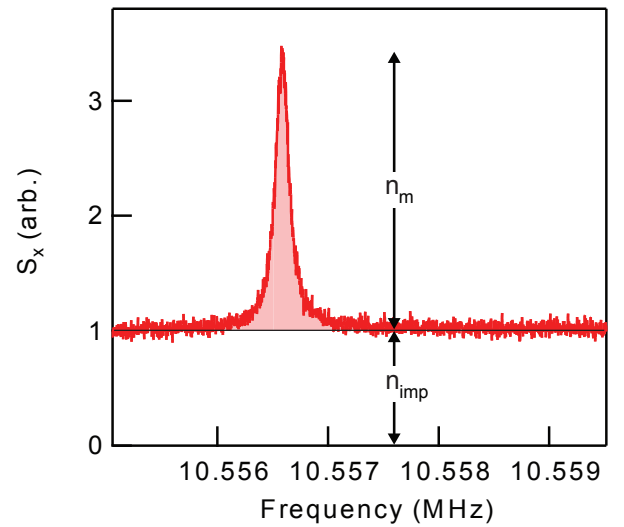


FIG. S4. Measurement imprecision in units of mechanical quanta.

our oscillator as $S_F^{\text{total}} = 4\hbar\Omega_m m\Gamma'_m(n_m + 1/2)$. As this total necessarily includes the backaction, we may make the most conservative assumption that it was solely due to backaction that our oscillator remained at finite occupancy. Hence, $n_{\text{ba}} \leq n_m + 1/2$. The low thermal occupancies attained in this work allow us to place an upper bound on how large the backaction could possibly be, and hence quantify our measurement in terms of approach to the Heisenberg limit. Thus, $\sqrt{S_x^{\text{imp}} S_F^{\text{ba}}} = 4\hbar\sqrt{n_{\text{imp}} n_{\text{ba}}} \leq 4\hbar\sqrt{n_{\text{imp}}(n_m + 1/2)}$. At $n_d = 3 \times 10^4$, we simultaneously achieve $n_m = 0.36$ and $n_{\text{imp}} = 1.9$ ($S_F^{\text{total}} = 1.6 \times 10^{-34}$ N²/Hz and $S_x^{\text{imp}} = 1.7 \times 10^{-33}$ m²/Hz) yielding an upper limit on the measured product of backaction and imprecision of $5.1 \hbar$. As stated above, the best possible backaction-imprecision product is $\hbar\sqrt{2}$ when using red-detuned excitation; thus our measurement is only a factor of 3.6 above this limit. It may also be noted that this factor would have been 1.8 except that our chosen geometry losses half of the signal back to the input ($\beta = 1/2$). In future experiments, using a single-port geometry ($\beta = 1$) will improve this inefficiency.

-
- [1] Walls, D. F. & Milburn, G. J. *Quantum Optics* (Springer, Berlin, 1994).
 [2] Marquardt, F., Chen, J. P., Clerk, A. A. & Girvin, S. M. Quantum theory of cavity-assisted sideband cooling of me-

- chanical motion. *Phys. Rev. Lett.* **99**, 093902 (2007).
 [3] Clerk, A. A., Devoret, M. H., Girvin, S. M., Marquardt, F. & Schoelkopf, R. J. Introduction to quantum noise, measurement, and amplification. *Rev. Mod. Phys.* **82**, 1155–1208 (2010).
 [4] Rocheleau, T. *et al.* Preparation and detection of a mechanical resonator near the ground state of motion. *Nature* **463**, 72–75 (2010).
 [5] Agarwal, G. A. & Huang, S. Electromagnetically induced transparency in mechanical effects of light. *Phys. Rev. A* **81**, 041803 (2010).
 [6] Weis, S. *et al.* Optomechanically Induced Transparency. *Science* **330**, 1520–1523 (2010).
 [7] Teufel, J. D. *et al.* Circuit cavity electromechanics in the strong-coupling regime. *Nature* **471**, 204–208 (2011).
 [8] Castellanos-Beltran, M. A., Irwin, K. D., Hilton, G. C., Vale, L. R. & Lehnert, K. W. Amplification and squeezing of quantum noise with a tunable Josephson metamaterial. *Nature Physics* **4**, 929–931 (2008).
 [9] Teufel, J. D., Donner, T., Castellanos-Beltran, M. A., Harlow, J. W. & Lehnert, K. W. Nanomechanical motion measured with an imprecision below that at the standard quantum limit. *Nature Nanotechnology* **4**, 820–823 (2009).
 [10] Dobrindt, J. M., Wilson-Rae, I. & Kippenberg, T. J. Parametric normal-mode splitting in cavity optomechanics. *Phys. Rev. Lett.* **101**, 263602 (2008).
 [11] Schliesser, A., Arcizet, O., Riviere, R., Anetsberger, G. & Kippenberg, T. J. Resolved-sideband cooling and position measurement of a micromechanical oscillator close to the Heisenberg uncertainty limit. *Nature Physics* **5**, 509–514 (2009).
 [12] Braginsky, V. B. & Khalili, F. Y. *Quantum Measurement* (Cambridge University Press, 1992).